RSC Advances

PAPER

View Article Online
View Journal | View Issue

Cite this: *RSC Adv.*, 2025, **15**, 29077

Light-triggered degradable bridged polysilsesquioxane nanoplatforms for spatiotemporally controlled drug release

Xin Zhang,[ab] Xiaonan Liu,[ab] Yutong Liu,[c] Xiaocen Wei,[b] Mengzhen Xing,[b] Lei Shi,[b] Linlin Zhang,[b] Yuning Ma,[b] Yuxia Ma[c] and Han Zhang*[d]

Developing stimuli-responsive nanoplatforms is a promising strategy for controlling the release of targeted molecules. In this study, nitrobenzyl ester was chosen as a photoresponsive moiety to functionalize an organic bridged linker, facilitating the synthesis of a photoresponsive silane, namely 2-nitro-1,3-phenyl bis(methylene mercaptoacetate ester) bridged trimethoxysilane (SMS). Light-triggered degradable bridged polysilsesquioxane nanoparticles (SMPS) were achieved through hydrolysis-condensation reactions using SMS as a precursor in suspension polymerization. Upon irradiation at 365 nm for three hours, the particle size of SMPS decreased from 138 ± 20 nm to 103 ± 43 nm. The target molecule, evodiamine (Evo), was efficiently loaded onto SMPS through hydrophobic and electrostatic attractions, constructing a light-controlled release system, Evo@SMPS. The results of *in vitro* experiments demonstrate that this photoresponsive platform exhibits effective light-triggered release behavior upon 365 nm. Under an irradiation intensity of 100 mW cm^{-2} for 12 hours, the cumulative release rate of Evo reached up to 92.3%, allowing precise control over the release amount, timing, and location of target molecules. This light-triggered degradable bridged polysilsesquioxane carrier platform with high biocompatibility holds significant potential and prospects for broad application in multifunctional controlled release systems.

Received 7th June 2025
Accepted 1st August 2025

DOI: 10.1039/d5ra04027b

rsc.li/rsc-advances

1 Introduction

Recent advancements in targeted drug delivery systems have been propelled by nanoparticles' remarkable drug-loading capacity, optimal stability, biocompatibility, and exceptional pharmacological properties.[1] These nanoparticles, typically composed of organic nanomaterials (*e.g.*, polymers, lipids),[2] inorganic materials (*e.g.*, metals, oxides, carbon),[3] and hybrid nanomaterials (*e.g.*, lipid-polymer, metal–organic hybrids),[4,5] possess submicron dimensions. These materials were designed and functionalized based on the specific properties and requirements of drugs or biomolecules, enabling efficient and safe controlled delivery.[6] Various external stimuli-triggered drug delivery systems have been developed to minimize off-target drug distribution and achieve precise, on-demand release.[7] Unlike endogenous stimuli such as redox, pH, and enzymes, exogenous stimuli like light, heat, magnetism, and ultrasound can be precisely controlled to allow spatial and temporal adjustments for targeted drug delivery.[8,9] Among them, light, a clean and non-invasive stimulus, has demonstrated superior potential for spatiotemporal controlled drug delivery.[10,11] Consequently, current research focuses on developing efficient light-triggered degradable strategies to construct photoresponsive and controllable delivery systems and promote their application in clinical medicine.

As a novel biomaterial formed from the synergistic combination of inorganic and organic constituents, bridged polysilsesquioxane (BPS) possesses exceptional biocompatibility, tunable dimensions, and tailored organic functional groups,[12] making it an ideal carrier for delivery, treatment, and diagnostic systems. However, issues such as degradation and long-term toxicity challenge the application of BPS. In order to address such problems, highly adaptable organic properties are employed to prepare BPS materials with specialized stimulus responsiveness.[13] These functional BPS materials can be utilized to construct controllable release systems, offering innovative materials and methodologies for precise diagnostics and treatments. For instance, novel pH-responsive biodegradable BPS nanoparticles with acetal bridged groups can contribute to the controlled release of anticancer drugs.[14] In reductive-responsive BPS systems, disulfide/tetrasulfide bonds,[15,16] diselenide bonds,[17] and ditelluride bonds[18] are commonly utilized as biodegradable

[a]*Shandong Key Laboratory of Digital Traditional Chinese Medicine, Shandong University of Traditional Chinese Medicine, Jinan 250355, China*
[b]*Institute of Pharmacy (Institute of TCM Health Industrial Technology), Shandong University of Traditional Chinese Medicine, Jinan 250355, China*
[c]*Department of Acupuncture and Massage College, Shandong University of Traditional Chinese Medicine, Jinan 250355, China*
[d]*Department of Pharmacy, Shandong University of Traditional Chinese Medicine, Jinan 250355, China. E-mail: 60030150@sdutcm.edu.cn*

organic bridges in carriers. These carriers degrade under high levels of glutathione (GSH), enhancing biodegradability and promoting target molecule release. The incorporation of thioacetal/ketone functionality introduces an oxidative response in BPS, leading to structure disruption and the degradation of its carrier by reactive oxygen species (ROS) in the biological environment, thereby facilitating on-demand drug release.[19,20] Oxalamide has been used as an organic bridged linker to prepare enzymatic degradable BPS nanoparticles.[21] Amide bonds cleave upon exposure to trypsin and degrade. A kind of photodegraded hollow mesoporous organosilicon nanoparticles was successfully synthesized. The singlet oxygen produced by graphene oxide quantum dots induces the cleavage of organic bridges, which in turn promotes the degradation of nanoparticles, thus significantly enhancing local drug release.[22] With photocleavage group 2-nitrobenzyl ester and diethylamino coumarin as side chain components of an organic bridged structure, the synthesized BPS materials display distinct charge inversion under light irradiation, allowing precise regulation of drug and bioactive molecule release.[23,24] However, they can only modify the surface properties of particles under light exposure, without enabling the carrier to degrade as a whole. Moreover, drug loading solely through electrostatic interactions results in low drug-loading capacity. Despite these advancements, BPS degradation often depends on high porosity or low organic content. Therefore, designing and preparing novel light-triggered degradable BPS particles is crucial for accelerating biodegradation and promoting target molecule release, which holds significant promise for advancing the clinical application of BPS-controlled release systems.

Evomine (Evo) is a natural active ingredient abundant in the traditional Chinese medicine Evodius officinus. Evo possesses pharmacological effects, such as analgesia, anti-inflammatory, anti-tumor, anti-microbial, cardiac protection, and regulation of metabolic diseases.[25] However, available data indicate that Evo has poor solubility in aqueous media, resulting in low bioavailability and severely limiting its therapeutic efficacy *in vivo*.[26,27] In this study, based on light-triggered degradable bridged polysilsesquioxane nanoparticles, a novel photoresponsive controlled release system (Evo@SMPS) was strategically designed and constructed for photomediated precise release of target molecules. The carrier platform demonstrates excellent stability in the absence of light and effectively prevents leakage of the loaded Evo. Upon exposure to light at a wavelength of 365 nm, the nitrobenzyl organic bridge was photocleaved, resulting in carrier photodegradation and the controlled release of target molecules. By optimizing illumination parameters, such as illumination intensity, duration, and on/off mode, this system allows accurate control over the release time, position, and dose of target molecules. The light-triggered degradable bridged polysilsesquioxane carrier platform exhibits extensive application potential in multifunctional controlled release systems.

2 Materials and methods

2.1 Materials and characterization

The 1,3-dimethyl-2-nitrobenzene (98%), chloroacetyl chloride (98%), and 3-mercaptopropyl trimethoxysilane (98%) were purchased from Shanghai Macklin Biochemical Technology Co., Ltd. The $BH_3\cdot THF$ solution (1.0 mol L^{-1}) was sourced from Anhui Zesheng Technology Co., Ltd. Potassium permanganate ($KMnO_4$) was obtained from Jinan Qiguang Technology and Trade Co., Ltd. Evomine (98%) was purchased from Xi'an Yatu Biotechnology Co., Ltd. CCK-8 kit was purchased from Beijing Solebo Technology Co., Ltd. All conventional inorganic solvents and organic solvents were obtained from Tianjin Fuyu Fine Chemical Co., Ltd.

Nuclear magnetic resonance (NMR) spectra were recorded on a Bruker Avance 400 MHz spectrometer by using DMSO-d_6 as the solvent. Ultraviolet-visible (UV-vis) absorption spectra were tested using the Agilent Cary 5000 UV-vis spectrometer. Fourier transform infrared (FTIR) spectra were recorded on a Bruker Tensor 27 spectrometer. Scanning electron microscope (SEM) images and transmission electron microscope (TEM) images were observed by Hitachi SU8010 scanning electron microscope and HT 7700 transmission electron microscope, respectively. The particle size distribution and zeta potential were measured by dynamic light scattering (DLS) using a Malvern Zetasizer Nano ZS90 system. The Agilent Model 1200 liquid chromatogram is used to determine high performance liquid chromatography (HPLC).

2.2 Synthesis of 2-nitro-1,3-benzenedicarboxylic acid

1,3-Dimethyl-2-nitrobenzene (1.51 g, 10.0 mmol), NaOH (0.64 g, 16.0 mmol), and DI water (80.0 mL) were fully mixed evenly, and KMnO4 (6.35 g, 40.0 mmol) was added in batches at 95 °C. After reacting for 24 h, HCl was slowly added to the filtrate under stirring until the solution pH = 2. The white product 2-nitro-1,3-benzenedicarboxylic acid was obtained by extraction and filtration (2.10 g, 96.0% yield). ^{1}H NMR (400 MHz, DMSO-d_6, δ ppm) 8.18 (d, J = 7.8 Hz, 2H), 7.82 (d, J = 7.9 Hz, 1H), 3.32 (s, 2H); ^{13}C NMR (101 MHz, DMSO-d_6, δ ppm) 164.82, 149.23, 135.16, 131.58, 125.27.

2.3 Synthesis of 2-nitro-1,3-benzenedimethanol

2-Nitro-1,3-benzenedicarboxylic acid (2.50 g, 11.8 mmol) was dissolved in anhydrous THF (20.0 mL). A solution of 1 M $BH_3\cdot THF$ (59 mL) was added dropwise to the above acid solution under ice bath. The reaction mixture was stirred at room temperature for 48 h. Excess methanol was slowly added until no more gas was produced. The resulting solution was evaporated, followed by redissolving in ethyl acetate. The organic phase was washed with $NaHCO_3$ saturated aqueous and DI water, then dried over anhydrous $MgSO_4$. The crude product was purified using column chromatography (*n*-hexane/ethyl acetate v/v = 1/1), yielding white product of 2-nitro-1, 3-benzenedimethanol (1.65 g, 76% yield). ^{1}H NMR (400 MHz, DMSO-d_6, δ ppm) 7.69–7.55 (m, 3H), 5.53 (t, J = 5.5 Hz, 2H), 4.59 (d, 4H); ^{13}C NMR (101 MHz, DMSO-d_6, δ ppm) 147.84, 135.12, 131.22, 128.40, 59.59.

2.4 Synthesis of 2-nitro-1,3-phenylene bis(methylene-2-chloroacetate)

2-Nitro-1,3-benzenedimethanol (1.10 g, 6.00 mmol) and triethylamine (1.20 g, 12.0 mmol) were dissolved in anhydrous

THF (25.0 mL). Chloroacetyl chloride (1.40 g, 12.0 mmol) was dissolved in anhydrous THF (15.0 mL) and added dropwise to the above mixture under ice bath. The reaction mixture was allowed to continue at room temperature for 24 h. After filtration and removal of the solvent by evaporation, the resulting sample was redissolved in ethyl acetate. The organic phase was washed three times with DI water and dried with anhydrous $MgSO_4$. The column chromatography (*n*-hexane/ethyl acetate v/v = 3/2) was used to purify the crude product, obtaining the white product 2-nitro-1, 3-phenylene bis(methylene-2-chloroacetate) (1.50 g, 74% yield). ^{1}H NMR (400 MHz, DMSO-d_6, δ ppm) 7.69–7.51 (m, 3H), 5.24 (s, 4H), 3.56 (m, 18H), 3.36 (m, 4H), 2.57 (t, 4H), 1.64 (m, 4H), 0.71 (m, 4H); ^{13}C NMR (101 MHz, DMSO-d_6, δ ppm) 172.27, 153.20, 137.20, 136.21, 134.21, 68.14, 45.84.

2.5 Synthesis of 2-nitro-1,3-phenyl bis(methylene mercaptoacetate ester) bridged trimethoxysilane

1.00 mmol of 2-nitro-1,3-phenylene bis(methylene-2-chloroacetate) was dissolved in MeCN, and then added with twice the amount of triethylamine and 3-mercaptopropyl trimethoxysilane. The reaction mixture was stirred at 60 °C under N_2 atmosphere for 6 h. After cooling to room temperature, the solvent was removed by rotary evaporation, and the residue was dissolved in anhydrous THF. The filtrate was evaporated to obtain an orange oily product, 2-nitro-1,3-phenyl bis(methylene mercaptoacetate ester) bridged trimethoxysilane (SMS, 82.0% yield). ^{1}H NMR (400 MHz, DMSO-d_6, δ ppm) 7.77–7.68 (m, 3H), 5.30 (s, 4H), 4.44 (d, J = 5.1 Hz, 4H); ^{13}C NMR (101 MHz, DMSO-d_6, δ ppm) 170.21, 148.51, 132.34, 130.84, 129.53, 67.48, 50.81, 35.12, 32.84, 25.59, 22.65; ^{29}Si NMR (79 MHz, DMSO-d_6, δ ppm) −45.95.

2.6 Preparation of bridged polysilsesquioxane nanoparticles

A catalyst solution of appropriate DI water and 1 M NaOH solution was added to a 50 mL round-bottom flask. Under 80 °C and 1500 rmp, the toluene solution containing monomer was added to the catalyst solution dropwise. After 8 hours of reaction, the samples collected by centrifugation were washed with EtOH and DI water. Bridged polysilsesquioxane nanoparticles (SMPS) were obtained by drying under vacuum at 60 °C.

2.7 Light-triggered degradation of SMS and SMPS

The DMSO-d_6 solution of SMS was placed at 5.00 cm below the light source (λ = 365 nm, 100 mW cm^{-2}). A certain amount of solution was taken out at various irradiation time for ^{1}H NMR spectra. The MeCN and EtOH solutions of SMS at 80.0 μg mL^{-1} were also irradiated using the same parameters to measure their UV-vis spectra.

The same irradiation parameters were used to irradiate SMPS suspension (1.00 mg mL^{-1} in DI water). 6.0 mL of solution was taken out at various irradiation time for UV-vis spectrum measurement.

2.8 *In vitro* cytotoxicity

HeLa cells were seeded in 96-well cell culture plates at 1×10^4 per well and incubated overnight in an incubator at 37 °C (5% CO_2), Subsequently, the cells were treated with SMPS (concentrations of 20, 50, 100, 200 μg mL^{-1}, light parameters of 12 h and 100 mW cm^{-2}) or Evo@SMPS (light intensities of 0, 20, 50, and 100 mW cm^{-2}, irradiation time of 12 h and concentration of 200 μg mL^{-1}) before and after irradiation. Following a 4-hours incubation period, the nanoparticles were removed. The cells were washed and transferred to fresh medium and then incubated at 37 °C for 24 h prior to the standard CCK-8 assay.

2.9 Drug loading and light-controlled release

Evo and SMS were dissolved in toluene to prepare a precursor solution containing the target molecule. A catalysis solution of appropriate DI water and 1 M NaOH solution was added to a 50 mL round-bottom flask, followed by the above toluene solution dropwise at 80 °C and 1500 rmp. The drug-loaded nanoparticles Evo@SMPS was collected by centrifugation after 8 h, and washed with EtOH and DI water, followed by drying in vacuum at 60 °C. The drug loading content (DLC) and drug loading efficiency (DLE) were calculated as follows:

$$\mathrm{DLC}(\%) = \frac{\text{Weight of Evo in Evo@SMPS}}{\text{Weight of Evo@SMPS}} \times 100\%$$

$$\mathrm{DLE}(\%) = \frac{\text{Weight of Evo in Evo@SMPS}}{\text{Weight of Evo in feed}} \times 100\%$$

A volume of 5.0 mL of Evo@SMPS suspension (1.0 mg mL^{-1} in PBS buffer solution) was placed in a dialysis bag (MWCO: 3.5 kDa) and immersed in 50.0 mL of PBS buffer solution, then shaken at 37 °C and 100 rpm in a shaking incubator. At specified time intervals, a 6.0 mL solution was taken out for measurement of Evo content using HPLC method. At the same time, add an equal amount of PBS buffer solution to ensure that the volume of the released liquid remains unchanged. All experiments were measured three times.

Two release conditions were set: (1) irradiation with light sources of intensities 0, 20, 50, and 100 mW cm^{-2} for 12 hours; (2) irradiation in ON/OFF mode (light on for 1 h and light off for 1 h) with light sources of intensities 20, 50, and 100 mW cm^{-2}. The cumulative release (%) of Evo was calculated as follows:

$$\mathrm{Cumulative}(\%) = \frac{\text{Weight of Evo in release solution}}{\text{Initial weight of Evo in Evo@SMPS}} \times 100\%$$

3 Results and discussion

3.1 Synthesis of photoresponsive bridged silane SMS

Nitrobenzyl ester was selected as the photoresponsive group for the functional design of the organic bridge. Meanwhile, the photoresponsive bridged silane SMS, namely 2-nitro-1,3-phenyl bis(methylene mercaptoacetate ester) bridged trimethoxysilane,

was synthesized for the first time using a simple, efficient, and mild preparation method. Fig. 1 illustrates the specific preparation steps and synthesis route of SMS. Starting with 1,3-dimethyl-2-nitrobenzene, benzyl group underwent oxidation and reduction to yield 2-nitro-1,3-benzenedimethanol, which was then occurred a substitution reaction with chloroacetyl chloride to generate 2-nitro-1,3-phenylene bis(methylene-2-chloroacetate). This was followed by a substitution reaction with twice the amount of 3-mercaptopropyl trimethoxysilane to produce the photoresponsive bridged silane SMS. The two endpoints of the photoresponsive functional unit nitrobenzyl ester formed a stable connection with thiol silane through a precisely designed covalent bond structure, integrating the photochemical activity of nitrobenzyl ester into the organic bridged main chain of silane at the molecular level. Subsequently, the photoresponsive properties of the bridged silane SMS were successfully achieved, laying a solid foundation for the further synthesis of bridged polysilsesquioxane nanoparticles with light-triggered degradation.

Fig. 2 details the ^{1}H NMR spectra of raw materials (a), intermediates (b–d), and SMS (e), clearly tracing the specific evolution of hydrogen protons in benzyl groups. For SMS, the chemical shifts of the three hydrogen protons Ha and Hb on the benzene ring are 7.69–7.51 ppm; the four benzyl hydrogen protons Hc have a chemical shift of 5.24 ppm; the chemical shifts of the hydrogen protons Hd, He, Hf, and Hg on the main chain methylene are 3.36, 2.57, 1.64, and 0.71 ppm, respectively; the chemical shift of the hydrogen proton Hh on the alkoxy group is 3.56 ppm. The chemical shifts of all the proton peaks of SMS have been assigned accurately, and the proportion of the integral area of each proton peak is consistent with the theoretical value, denoting the successful synthesis of the photoresponsive bridged silane SMS.

3.2 Photoresponsive behaviour of the bridged silane SMS

Fig. 3(a) illustrates the photolysis process of the bridged silane SMS in detail. The photoresponsive functional unit of SMS is the nitrobenzyl ester group, which undergoes electronic transition under 365 nm photoexcitation, leading to a series of charge rearrangement reactions within the molecule. Finally, the C–O bond in nitrobenzyl ester is broken to produce 2-nitrosobenzaldehyde thioacetate siloxane and 3-(trimethoxysilyl propyl) thioacetic acid. The specific photolysis mechanism is as follows: after the nitro group ($-NO_2$) on the *o*-nitrobenzyl moiety absorbs a 365 nm photon, an n → π* transition occurs, promoting the molecule to the singlet excited state. The excited nitro group abstracts an electron from the adjacent benzylic C–H bond, initiating an intramolecular single electron transfer. The electron pair on the ester oxygen atom then shifts towards the benzylic carbon, resulting in the heterolytic cleavage of the C–O bond between the benzylic carbon and ester oxygen atom. The highly unstable $+CH^-$ immediately undergoes an intramolecular reaction with the adjacent nitroso oxygen atom (–N=O), forming a five-membered ring intermediate. This intermediate is unstable and rapidly decomposes into 2-nitrosobenzaldehyde thioacetate siloxane and 3-(trimethoxysilylpropyl) thioacetic acid.

The photoresponsive behavior of the bridged silane SMS in the DMSO-d_6 solution was monitored using ^{1}H NMR spectra (Fig. 3(b)). After 30 minutes of 365 nm light irradiation, the signal of $PhCH_2^-$ at the chemical shift c' (δ = 5.24 ppm) gradually weakened. The proton's peak area decreased from 4.00 to 2.94. With continued irradiation, it further dropped. After 60 minutes of illumination, the peak area of $PhCH_2^-$ at c' was 2.71. This is because the photocleavage reaction of the nitrobenzyl ester group in SMS causes the consumption of the benzyl group. According to the relative change in the proton's peak area at $\delta = 5.24$ ppm, the photodegradation degree of SMS can reach 32.3% upon 60 minutes of 365 nm monomer solution irradiation. Simultaneously, new absorption peaks appeared at 3.47 ppm and 3.33 ppm, assigned to the methylene protons (d′) in 2-nitrosobenzaldehyde thioacetate siloxane and the methylene protons (d″) in 3-(trimethoxysilylpropyl) thioacetic acid, respectively. These changes in the ^{1}H NMR spectrum of the solution after illumination demonstrate the photolysis reaction of SMS.

The photodegradation of SMS in MeCN and EtOH solutions was tracked using UV-vis absorption spectroscopy. As shown in Fig. 4(a), under 365 nm light irradiation, the MeCN solution of SMS develops a new characteristic absorption peak at 308 nm, which intensifies with irradiation duration. The absorption peak arises from the n → π* electron transition of the 2-nitrosobenzaldehyde group in the photolysis product, indicating that the bridged silane SMS is photoresponsive. Fig. 4(b) displays the UV-vis absorption spectra of SMS in EtOH solution after photoreaction. Due to solvation, the UV-vis absorption of SMS differs between EtOH and MeCN solutions. The black line (0 min) represents the UV-vis absorption spectrum of unreacted

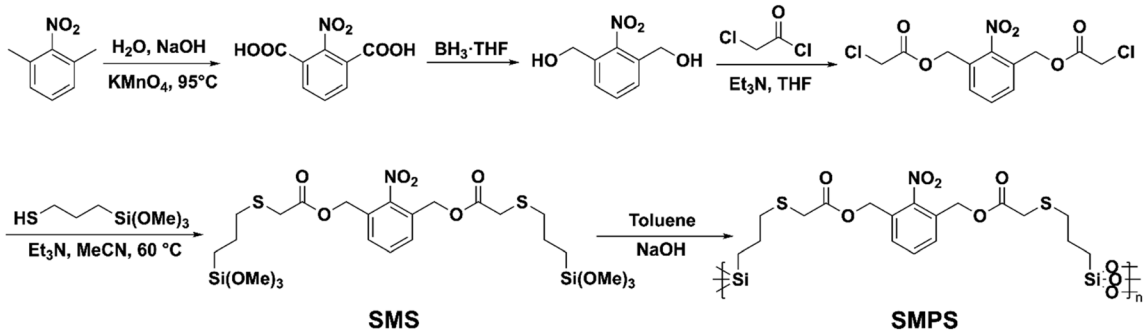

Fig. 1 Synthetic routes for photoresponsive bridged silane SMS and light-triggered degradable bridged polysilsesquioxane SMPS.

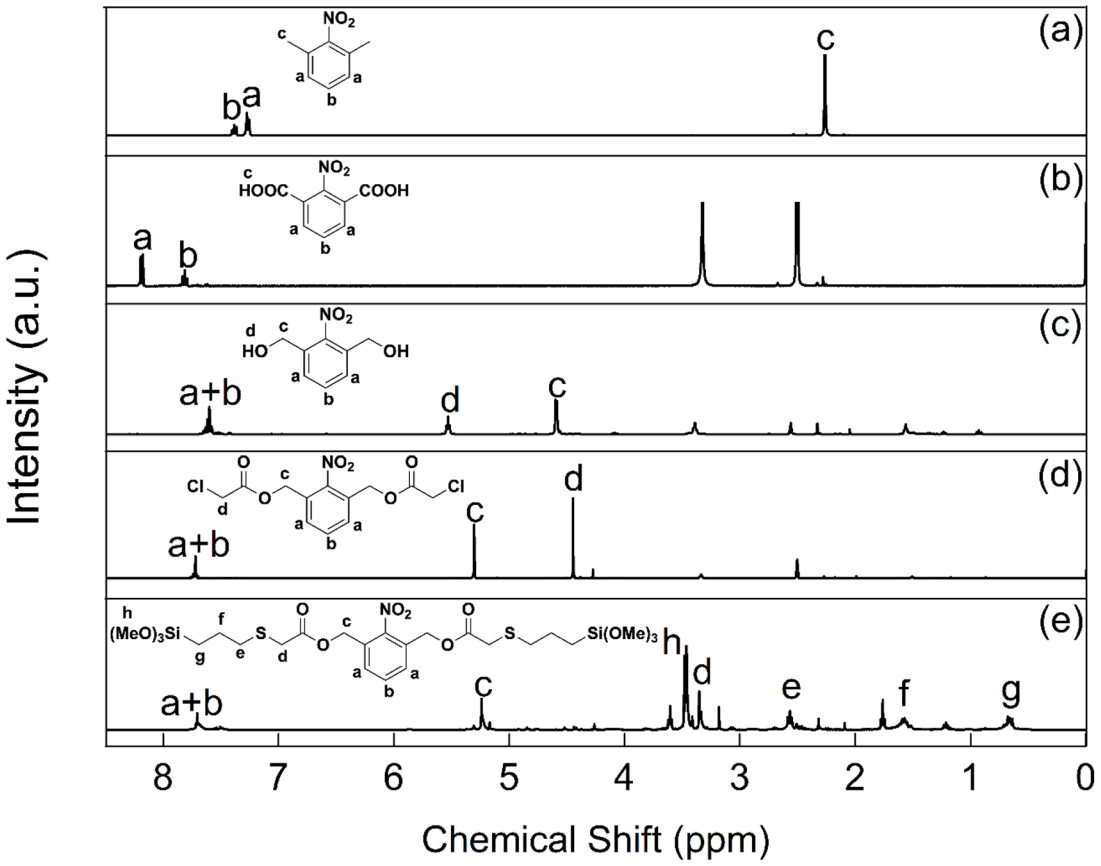

Fig. 2 ^{1}H NMR comparison of 1,3-dimethyl-2-nitrobenzene (a), 2-nitro-1,3-benzenedicarboxylic acid (b), 2-nitro-1,3-benzenedimethanol (c), 2-nitro-1,3-phenylene bis(methylene-2-chloroacetate) (d), and photoresponsive bridged silane SMS (e).

SMS in the EtOH solution. In the spectrum, a characteristic absorption peak resulting from the n → π* electron transition between the nitro and ester groups occurs at 237 nm. Another characteristic absorption peak appears at 204 nm, which is attributed to the π → π* electron transition of the phenyl group. Through illumination, a new absorption peak emerges at 312 nm, arising from the n → π* electron transition between nitroso and aldehyde groups. Its peak area grows with illumination time, owing to the production of 2-nitrobenzaldehyde siloxane monomer in the photocleavage reaction of SMS. Upon irradiation in EtOH, the absorption peak at 204 nm blueshifts to 208 nm arising from the conversion of nitro (–NO_2) to nitroso (–NO). The disruption of the phenyl ring's extended conjugation system due to photolytic cleavage of the N–O bond in the nitro group. The bond cleavage isolates the phenyl moiety, increasing its HOMO–LUMO gap and thus requiring higher energy (shorter wavelength) for the π → π* transition. Meanwhile, the ratio of peak areas between the absorption peaks at 237 nm and 204 nm declines progressively, reflecting the consumption of the nitro and ester groups in SMS. These findings confirm the photoresponsive behaviour of SMS under 365 nm light irradiation.

3.3 Light-triggered degradation behaviour of SMPS

3.3.1 Morphology characterization. A suspension polymerization method with the bridged silane SMS as the sole silicon source and toluene as the organic solvent template was employed to prepare light-triggered degradable bridged polysilsesquioxane nanoparticles. The specific steps are as follows: under a constant temperature of 80 °C and a rotational speed of 1500 rpm, a toluene solution containing SMS monomer was added dropwise to 1 M sodium hydroxide aqueous solution for 12 hours. Then, the underlying solids were collected, separated *via* ultrasonic treatment, centrifugated, and washed. Finally, the obtained solids were dried under vacuum at 60 °C to yield a light-yellow powder, the bridged polysilsesquioxane SMPS nanoparticles. The morphology of SMPS nanoparticles was observed and analyzed by SEM, as shown in Fig. 5(a). SMPS nanoparticles exhibit complete sphericity and a relatively uniform size distribution with minimal variation. In addition, the surface of the nanoparticles presents a slightly rough texture, which may be due to irregular clustering during formation.

In order to further investigate the light-triggered degradation behaviour of SMPS nanoparticles, a special light source with a wavelength of 365 nm and an intensity of 100 mW cm^{-2} was selected to irradiate SMPS nanoparticles uniformly dispersed in aqueous solution. SEM observation was conducted following one hour and three hours of irradiation. The observed SEM images in Fig. 5(b) and (c) display significant morphological changes in the SMPS nanoparticles. After one hour of

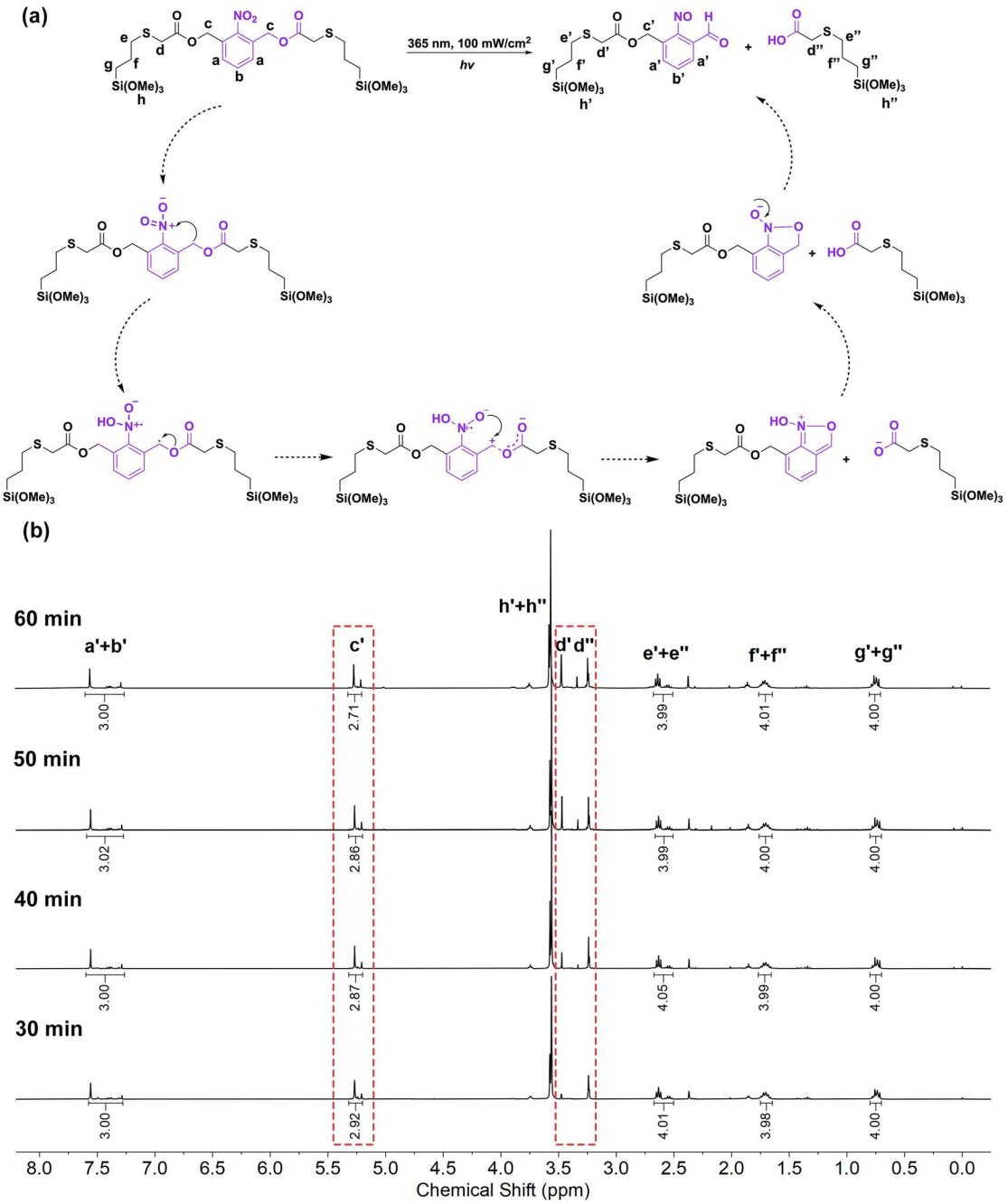

Fig. 3 (a) Photolysis mechanism of bridged silane SMS upon 365 nm UV light. (b) ^{1}H NMR spectrum for different time durations under irradiation.

illumination, the nanoparticles transition from the initial regular spherical shape to an ellipsoid shape. Upon three hours of exposure, the nanoparticles further evolve into irregular spherical structures. It is speculated that the light-triggered degradation process of nanoparticles has three stages. First, in the initial stage of light stimulation, the photoresponsive groups on the microsphere surface are degraded, and the molecular structures are gradually destroyed, forming holes and cracks and reducing the volume of the microsphere. Second, with the progress of degradation, the internal structure of the nanoparticles is exposed, causing changes in the internal pore structure and resulting in an irregular spherical shape. Finally, the nanoparticles degrade completely into small fragments or particles. Besides the photodegradation of photoresponsive groups, this process may also be accompanied by chemical reactions, such as ester bond and silico–oxygen bond hydrolysis in organic bridges.

Moreover, dynamic light scattering (DLS) was adopted to analyze changes in the particle size of SMPS nanoparticles through illumination. Fig. 6(a) depicts that the particle size decreases from 138 ± 20 nm to 103 ± 43 nm after three hours of illumination, indicating the occurrence of light-triggered SMPS degradation.

3.3.2 UV-vis absorption spectrum. In order to explore the light-triggered degradation behaviour of SMPS nanoparticles, the

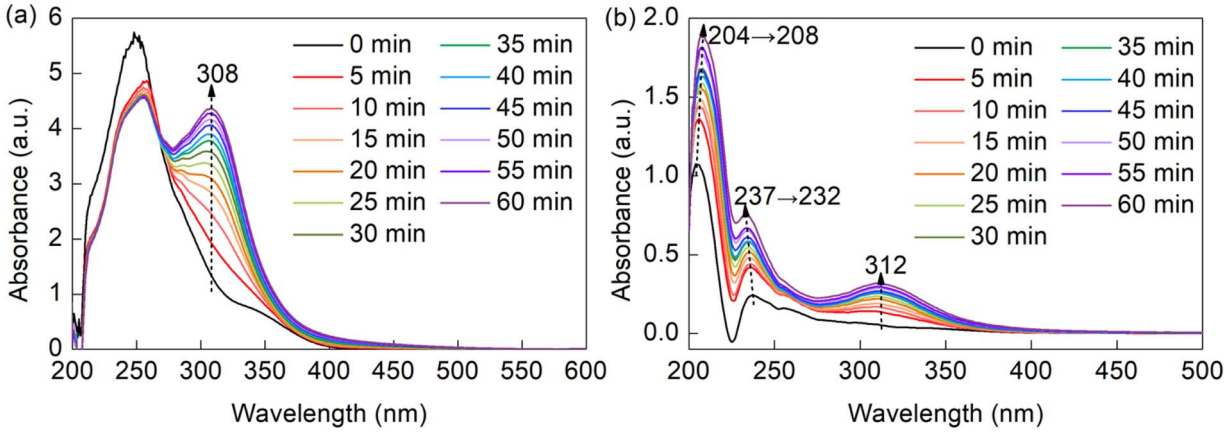

Fig. 4 UV-vis spectra of SMS in MeCN (a) and EtOH (b) solution upon 365 nm irradiation.

nanoparticles were uniformly dispersed in an aqueous solution with a pH of 7.0, undergoing the irradiation of a light source (a wavelength of 365 nm and an intensity of 100 mW cm^{-2}) for various durations. The UV-vis absorption spectrum was used to monitor SMPS dispersion, as shown in Fig. 6(b). The dispersion of SMPS after exposure was centrifuged, and the supernatant was collected for UV-vis absorption analysis. Under irradiation, an absorption peak of the solution appears at 310 nm, and the absorbance increases with irradiation time. The characteristic absorption peak at 310 nm corresponds to the n → π* electron transition between nitro and aldehyde groups of the photolysis products. This implies that SMPS is photoresponsive.

3.4 Drug loading of Evo@SMPS

Evo was used as the target molecular model of traditional Chinese medicine to develop an efficient delivery system. Suspension polymerization was employed to construct a light-controlled release system (Evo@SMPS) with light-triggered degradable SMPS nanoparticles as the carrier. In this process, photoresponsive bridged silane SMS was selected as the monomer, and toluene served as the organic solvent, establishing a suitable chemical reaction environment. NaOH was introduced as an alkaline catalyst to promote the reaction rate of the silane monomer during hydrolytic condensation. As the silane monomer was hydrolyzed and condensed to form the nanoparticles, the target Evo was encapsulated in the matrix of the nanoparticles through hydrophobic and electrostatic interactions, ensuring efficient loading and stable release of the target molecules. Such a design not only improves the bioavailability of target molecules but also guarantees light-triggered release, offering significant implications for delivery system development.

In the suspension solution, the silane monomer and target molecules form a uniform oil phase solution under the dissolution of toluene. Through intense agitation, this oil phase solution is dispersed as small droplets in the water phase system. Under the action of the alkaline catalyst, the silane monomer in the droplets undergoes hydrolysis and condensation at the oil–water interface. The hydrolysis of siloxane groups produces abundant hydrophilic silicyl groups, which extend outwards into the water. Meanwhile, the organic bridged group connected with silicon atoms in the monomer extends inward to the oil phase due to its hydrophobicity, resulting in the self-emulsification of the droplets with silicon hydroxyl groups on the surface. This effect ensures stable suspension of oil phase droplets in the water phase system. As hydrolytic polycondensation progresses, the monomer inside the droplets continues to migrate to the oil–water interface and reacts to build a Si–O–Si cross-linked shell with a three-dimensional network structure. The oil-phase toluene is co-wrapped within the nanoparticles as a solvent nucleus along with the target molecules. As toluene evaporates, the target molecules remain

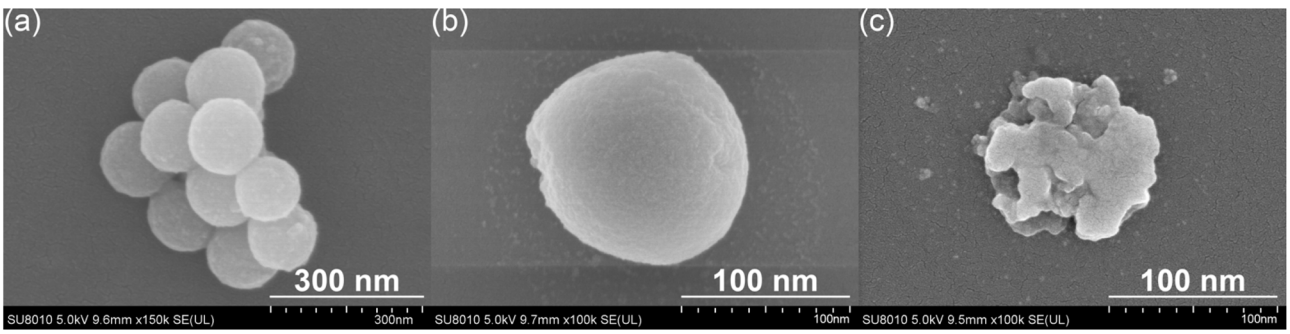

Fig. 5 Morphological changes of SMPS nanoparticles after 0 h (a), 1 h (b) and 3 h (c) of 365 nm irradiation observed by SEM.

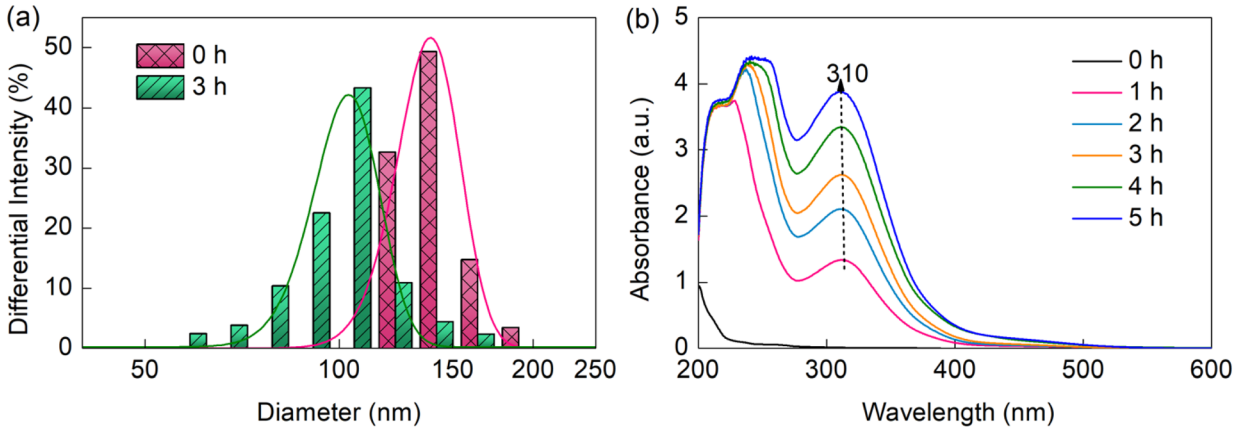

Fig. 6 (a) DLS measurements of changes in size distribution of SMPS nanoparticles after different irradiation durations. (b) UV-vis spectra of SMPS nanoparticles upon 365 nm for different irradiation durations.

within the microsphere matrix, realizing the inclusion of these molecules. Additionally, Evo, along with toluene, is free in the water phase. Due to its low water solubility and positive charge, Evo is attracted and attached to the surface of negatively charged nanoparticles under electrostatic interactions. Ultimately, light-triggered degradable bridged polysilsesquioxane nanoplatforms are obtained.

The quality and performance of the prepared nanoparticles were evaluated using various methods. HPLC was adopted to determine drug loading amount and rate. The morphology of nanoparticles was observed by SEM and TEM. The zeta potential and particle size distribution were measured *via* DLS. The drug release performance and stability of the nanoparticles under varying irradiation parameters were evaluated by *in vitro* release experiments.

First, a standard solution of Evo in methanol with gradient concentrations was prepared for HPLC analysis. Then, a standard curve was drawn with the peak area as the vertical coordinate and the concentration as the horizontal coordinate (Fig. 7(a)). Linear regression analysis yielded the equation $A = 85\,647C + 251\,171$ and a standard variance $R^2 = 0.99934$, demonstrating a strong linear relationship between the concentration of Evo and the peak area. Where C denotes the concentration of Evo in μg mL^{-1}, and A represents the peak area in mV min^{-1}. This equation can be used to derive Evo content in solutions with unknown concentrations.

By adjusting the dosage ratio R ($R = w$(SMS): w(Evo)), a series of Evo@SMPS nanoparticles containing different drug loads were prepared. Fig. 7(b) illustrates the drug-loading capacity (DLC) and efficiency (DLE) of these nanoparticles. Corresponding to the R of 1, 3, 5, and 7, the DLC of Evo@SMPS decreases progressively from 15.4% to 11.9%, 10.2%, and 9.50%. Conversely, DLE increases with R (indicating a decrease of Evo feeding proportion), rising from 51.2% to 58.6%, 67.9%, and 73.1%. DLC and DLE directly impact the release efficiency and effectiveness of target molecules, making them crucial indicators of Evo@SMPS carrier. Therefore, it is necessary to select appropriate drug-loading capacity and efficiency. Although reducing the dosage of Evo feeding decreases DLC, it may enhance the evenness and efficiency of target molecules, thereby promoting their bioavailability and therapeutic efficacy.

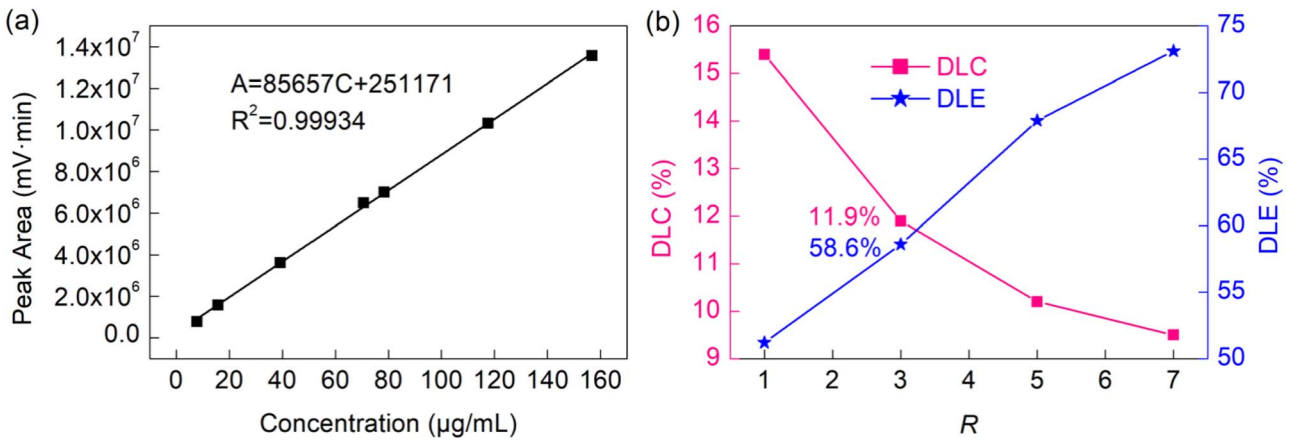

Fig. 7 (a) Standard calibration curve of the target molecule Evo in methanol solution. (b) Drug loading content and efficiency of Evo@SMPS with different R.

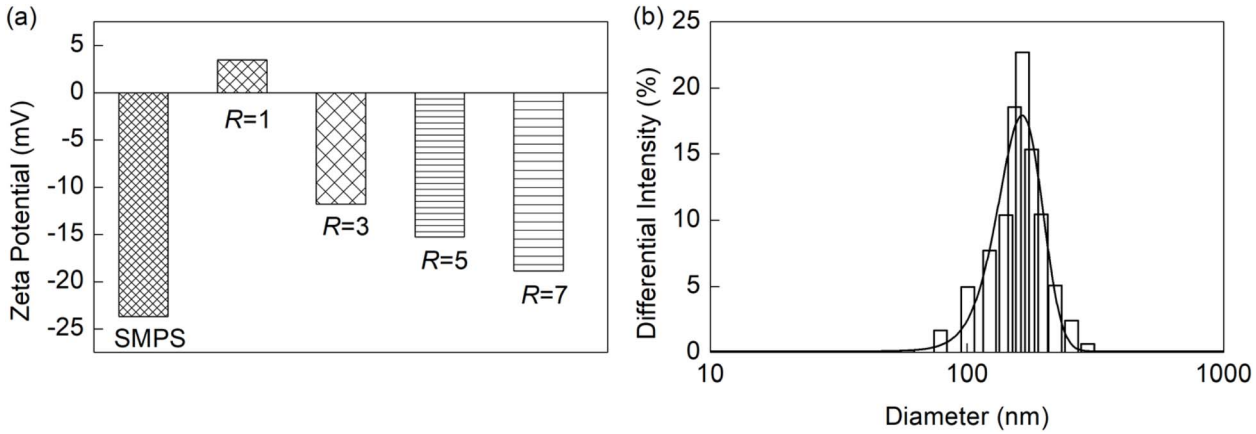

Fig. 8 (a) Zeta potential of Evo@SMPS prepared with different R in PBS buffer solution. (b) The size distribution of Evo@SMPS when $R = 3$.

Fig. 8(a) shows changes in the surface potential of Evo@SMPS nanoparticles with varying R in a PBS buffer solution. In the absence of drug loading, the surface potential of SMPS nanoparticles is −23.7 mV. For Evo@SMPS nanoparticles, the surface potential decreases with R. When $R = 1$, the surface charge of Evo@SMPS reverses from negative to positive, reaching +3.46 mV. This is due to the high feeding ratio of Evo, in which some Evo molecules are encapsulated within the nanoparticles during formation, and others adhere to the microsphere surface under electrostatic interactions, thus reversing the surface charge.

Furthermore, when R increases to 3, 5, and 7, the surface potentials of Evo@SMPS remain negative, which are −11.78 mV, −15.3 mV, and −18.9 mV. Previous studies have shown that negatively charged drug delivery systems facilitate blood circulation because they are not easily taken up by cells, thus prolonging circulation time in the body. Considering key indicators such as DLC, DLE, and zeta potential, Evo@SMPS obtained at $R = 3$ is optimal for further study, showcasing the advantages and suitability of drug-loaded system.

Fig. 8(b) presents the particle size distribution of Evo@SMPS nanoparticles with $R = 3$, whose particle size is 164.59 ± 62.25 nm. The SEM images in Fig. 9(a) show that Evo@SMPS at $R = 3$ have a regular spherical morphology, with a slightly rough surface and good dispersion. TEM images in Fig. 9(b) further reveal the internal structure of the nanoparticles. The target molecules are uniformly wrapped in the polysilsesquioxane matrix, forming a consistent and stable drug-loaded system.

By precisely adjusting the input ratio of the bridged silane monomer to the target molecules, the physical and chemical properties of the drug-loaded system can be optimized, including drug-loading capacity and efficiency, surface potential, and particle size distribution. This strategy lays a robust scientific foundation for building efficient, safe, accurate, and personalized controllable release platforms.

3.5 Light-controlled release of Evo@SMPS

Evo@SMPS was designed to induce carrier degradation through light irradiation, thereby precisely controlling the release of target molecules. Drug-loaded Evo@SMPS nanoparticles were dispersed in a PBS buffer solution to validate their characteristics. Following a predetermined irradiation interval, the Evo content in the solution was identified using HPLC. In order to systematically investigate the effects of different light parameters on the release of target molecules, two experimental schemes were designed: (a) irradiation with four light

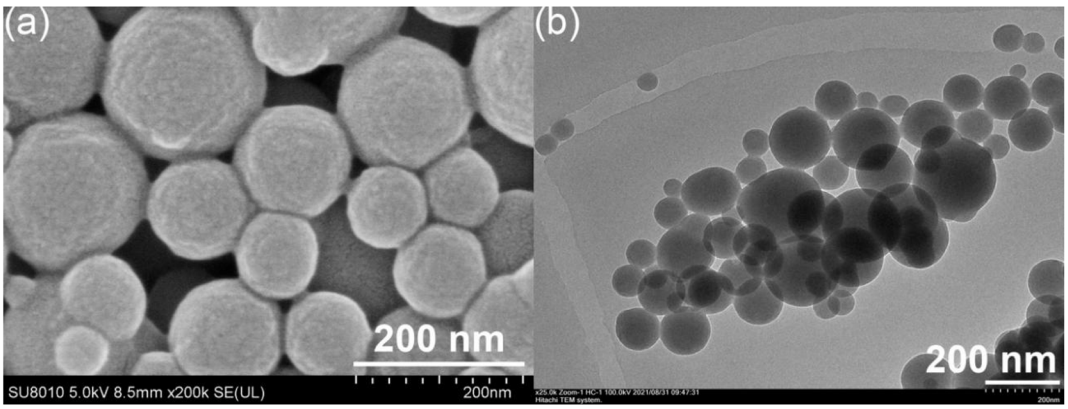

Fig. 9 SEM (a) and TEM (b) images of Evo@SMPS at $R = 3$.

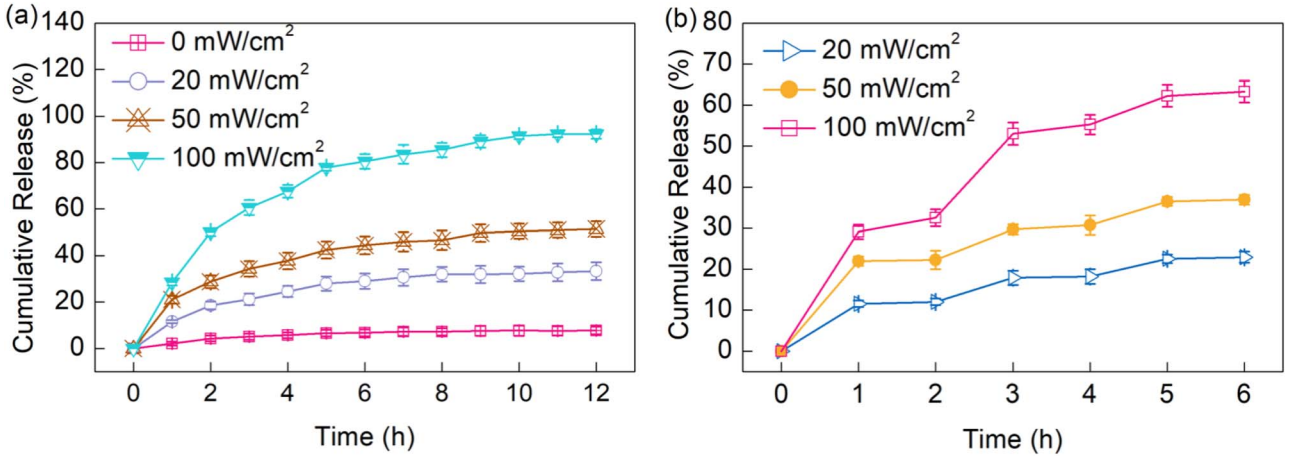

Fig. 10 The light-controlled release profile of Evo@SMPS under continuous irradiation mode (a) and under ON/OFF cyclic irradiation mode (b).

intensities (0, 20, 50, and 100 mW cm^{-2}) for 12 hours; (b) an ON/OFF irradiation mode (*i.e.*, the light source is alternated on and off each hour, totaling six cycles) with 20, 50, and 100 mW cm^{-2} intensities. Fig. 10(a) presents the curves of target molecules released by the Evo@SMPS carrier platform under varying light intensities. In the absence of external light stimulation (0 mW cm^{-2}), the system only released approximately 5% of Evo within three hours, and the total release remained below 8% within 12 hours, demonstrating the excellent stability and reliability of the controlled release system. When exposed to light, the target molecules were quickly released from the carrier, indicating that the system's release behaviour hinges on light stimulation.

A 365 nm light source was used to irradiate the Evo@SMPS solution, triggering the release of target molecules. The light stimulation initiates the photocleavage of the SMPS carrier, facilitating Evo release. Due to the convenience and precision of light stimulation, target molecule release can be precisely regulated. At a light intensity of 20 mW cm^{-2} for 12 hours of irradiation, about 33.3% of the target molecules were successfully released. When the light intensity was increased to 50 mW cm^{-2}, the cumulative release rate of Evo elevated to 51.4%. Further increasing the light intensity to 100 mW cm^{-2} achieved a cumulative release rate of Evo@SMPS as high as 92.3%. The results verify the satisfying light-controlled release behavior of the Evo@SMPS system, and the cumulative release rate of target molecules can be accurately controlled through light intensity modulation. In the initial stage of light-controlled release (within the first two hours of illumination), the release rate of Evo is relatively high, which may be attributed to the fact that the light-triggered degradation process of SMPS begins on the microsphere surface, leading to the preferential release of Evo adsorbed on the carrier surface.

Fig. 10(b) depicts the release profile of Evo from the Evo@SMPS system when the light source (20, 50, and 100 mW cm^{-2}) is alternated "ON" and "OFF" every two hours. The cumulative release rate of Evo increases when the light source is "ON" and nearly ceases when the light source is "OFF", showing a sensitive light-triggered release feature. The experimental results confirm that the release of target molecules from the Evo@SMPS system can be precisely adjusted under light stimulation.

3.6 *In vitro* cytotoxicity

To evaluate the biosafety of light-responsive SMPS nanoparticles for potential biomedical applications, we conducted a systematic assessment of their cytocompatibility and

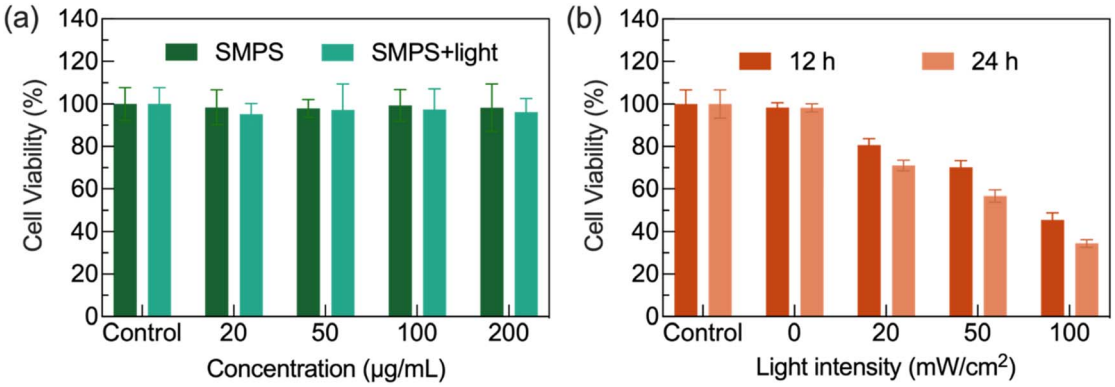

Fig. 11 (a) Cell viabilities of HeLa cells incubated with different concentrations of SMPS without and with irradiation. (b) Cell viabilities of HeLa cells incubated with different incubation periods of Evo@SMPS under different light intensities.

photodegradation byproducts. HeLa cells were exposed to pristine SMPS nanoparticles or UV-irradiated particles (SMPS-light, 12 h UV treatment) at concentrations ranging from 20 to 200 μg mL^{-1} for 24 h. Cellular viability was quantified using the CCK-8 assay under both light and dark conditions. As demonstrated in Fig. 11(a), neither pristine SMPS nor photodegraded particles exhibited significant cytotoxicity across the tested concentration spectrum. Cellular viability consistently remained above 95% throughout the observation period, with no statistically significant differences observed between treatment groups. These findings substantiate the exceptional biocompatibility of this photo-responsive drug delivery nanoplatform, meeting essential requirements for therapeutic applications.

In addition, we explored the cytotoxicity of the drug-loaded nanoplatform Evo@SMPS and examined its effect after irradiation at different light intensities (0, 20, 50, 100 mW cm^{-2}) for incubation with HeLa cells. Degradation of Evo@SMPS under light irradiation led to leakage of the loaded drug at the molecular level, which in turn triggered the destruction of tumor cells. As shown in Fig. 11(b), the cytotoxicity of irradiated Evo@SMPS on cancer cells was significantly enhanced with increasing light intensity and prolonged incubation time compared to unirradiated (0 mW cm^{-2}) Evo@SMPS. This result further confirms that a spatiotemporally controlled release and significant accumulation of Evo in the cells was achieved due to the light-triggered degradation of SMPS.

4 Conclusions

With the photocleavage group nitrobenzyl ester as the photoresponsive unit, the organic bridge was functionally designed at the molecular level, imparting photoresponsive characteristics to the bridged silane SMS. The SMPS nanoparticles, prepared *via* suspension polymerization using SMS as the sole silicon source, exhibit good dispersion and a uniform solid structure. After being exposed to light at 365 nm for three hours, the light-triggered degradation of the nanoparticles reduced the particle size from an initial 138 ± 20 nm to 103 ± 43 nm. The Evo@SMPS light-controlled release system achieves efficient loading and stable release of the target molecules by regulating the input ratio of SMS to Evo. Evo's bioavailability is promoted. The release behaviour of this carrier platform is effectively triggered by 365 nm light stimulation, and the release amount, timing, and location of the target molecules can be precisely regulated by adjusting irradiation parameters. The highest cumulative release rate attained is 92.3%. The Evo@SMPS light-controlled release system is characterized by high efficiency, safety, precision, and customization, offering a robust scientific foundation and broad application potential for controlled drug delivery platforms.

Author contributions

Xin Zhang: methodology, formal analysis, visualization, and writing – original draft. Xiaonan Liu: methodology, formal analysis, and visualization. Yutong Liu: investigation and data curation. Xiaocen Wei: methodology and data curation. Mengzhen Xing: formal analysis and visualization. Lei Shi: formal analysis and validation. Linlin Zhang: formal analysis and investigation. Yuning Ma: conceptualization and supervision. Yuxia Ma: conceptualization and supervision. Han Zhang: funding acquisition and writing – review and editing.

Conflicts of interest

There are no conflicts to declare.

Data availability

All data supporting the findings of this study are included within the manuscript.

Acknowledgements

This research was funded by the National Natural Science Foundation of China (No. 8240132197), the Shandong Provincial Natural Science Foundation (No. ZR2023QB236 and ZR2023QB199), the Shandong Provincial Development Plan for Youth Innovation Team in Higher Education Institution (No. 2023KJ347), the Shandong Provincial Medical Health Science and Technology Project (No. 202213050519 and 202213020603), the Shandong Provincial Traditional Chinese Medicine Science and Technology Project (No. Q-2023108), and the Scientific Research Funding Project of the Shandong University of Traditional Chinese Medicine (No. KYZK2024Q09). The authors gratefully acknowledge the postdoctoral program of the Shandong University of Traditional Chinese Medicine.

Notes and references

1 L. Eltaib, *Polymers*, 2025, **17**, 833.
2 B. Z. Chen, Y. T. He, Z. Q. Zhao, Y. H. Feng, L. Liang, J. Peng, C. Y. Yang, H. Uyama, M.-A. Shahbazi and X. D. Guo, *Adv. Drug Delivery Rev.*, 2023, **203**, 115109.
3 Q. Tan, S. Zhao, T. Xu, Q. Wang, M. Zhang, L. Yan, X. Chen and M. Lan, *Coord. Chem. Rev.*, 2023, **494**, 215344.
4 G. Kabay, A. E. Meydan, T. Eom, B. S. Shim, M. Mutlu and G. Kaleli-Can, *Int. J. Pharm.*, 2023, **630**, 122442.
5 T. M. Sampath Udeni Gunathilake, Y. C. Ching, C. H. Chuah, N. A. Rahman and N.-S. Liou, *Int. J. Biol. Macromol.*, 2020, **158**, 670–688.
6 F. Moradi Kashkooli, M. Soltani and M. Souri, *J. Controlled Release*, 2020, **327**, 316–349.
7 M. Fatima, W. H. Almalki, T. Khan, A. Sahebkar and P. Kesharwani, *Adv. Mater.*, 2024, **36**, 2312939.
8 J. Liao, J. Sun, W. Jia, W. He, H. Wang, W. Huang, Y. Wang, M. Yu, Y. Xie and Y. Chen, *Chem. Commun.*, 2025, **61**, 3946–3966.
9 S. E. Alavi, S. Alharthi, S. Z. Alavi, A. Raza and H. Ebrahimi Shahmabadi, *Drug Discovery Today*, 2024, **29**, 103849.
10 Y. Yang, K. Long, Y. Chu, H. Lu, W. Wang and C. Zhan, *Adv. Funct. Mater.*, 2024, **34**, 2402975.

11 J. Liu, W. Kang and W. Wang, *Photochem. Photobiol.*, 2022, **98**, 288–302.
12 X. Zhang, H. Zhang, X. Liu, J. Wang, S. Li and P. Gao, *Polymers*, 2024, **16**, 3163.
13 R. S. Guimarães, C. F. Rodrigues, A. F. Moreira and I. J. Correia, *Pharmacol. Res.*, 2020, **155**, 104742.
14 S. Yang, J. Fan, S. Lin, Y. Wang and C. Liu, *Colloids Surf., A*, 2020, **585**, 124133.
15 S. Shahbaz, M. Esmaeili, M. H. Fathian Nasab, Z. Imani, R. Bafkary, M. Amini, F. Atyabi and R. Dinarvand, *Int. J. Pharm.*, 2024, **655**, 124024.
16 D. Jiang, X. Xia, Z. He, Y. Xue and X. Xiang, *J. Ind. Eng. Chem.*, 2023, **123**, 382–395.
17 Q. Shen, M. Cao, C. Yu, J. Tang, L. Song, Y. Ding, L. Ju, J.-F. Wei, L. Li and W. Huang, *ACS Nano*, 2024, **18**, 16934–16946.
18 X. Xia, J. Shi, Q. Deng, N. Xu, F. Huang and X. Xiang, *Mater. Today Chem.*, 2022, **23**, 100660.
19 Z. Lin, L. Xu, J. Zhang, Z. Li and J. Zhao, *Nano*, 2019, **14**, 1950141.
20 Y. Yu, J. Chen, S. Liu and D. Cheng, *J. Mater. Chem. B*, 2021, **9**, 6044–6055.
21 J. G. Croissant, Y. Fatieiev, K. Julfakyan, J. Lu, A.-H. Emwas, D. H. Anjum, H. Omar, F. Tamanoi, J. I. Zink and N. M. Khashab, *Chem.–Eur. J.*, 2016, **22**, 14806–14811.
22 J. Fan, Z. Zhang, Y. Wang, S. Lin and S. Yang, *J. Nanobiotechnol.*, 2020, **18**, 91.
23 X. Zhang, M. Zhang, M. Wu, L. Yang, R. Liu, R. Zhang, T. Zhao, C. Song, G. Liu and Q. Zhu, *Polymers*, 2021, **13**, 2392.
24 X. Zhang, M. Zhang, M. Wu, L. Yang, R. Liu, R. Zhang, T. Zhao, C. Song, G. Liu and Q. Zhu, *ACS Appl. Mater. Interfaces*, 2021, **13**, 36370–36379.
25 Q. Sun, L. Xie, J. Song and X. Li, *J. Ethnopharmacol*, 2020, **262**, 113164.
26 Y.-N. Zhang, Y.-F. Yang and X.-W. Yang, *Biomed. Pharmacother.*, 2018, **98**, 82–87.
27 R. Solanki, A. K. Jangid, M. Jadav, H. Kulhari and S. Patel, *Macromol. Biosci.*, 2023, **23**, e2300077.